33RD CONGRESS
OF THE INTERNATIONAL COUNCIL
OF THE AERONAUTICAL SCIENCES
STOCKHOLM, SWEDEN, 4-9 SEPTEMBER, 2022

ICAS 2022 SWEDEN

IDENTIFICATION OF CRITICAL ACOUSTIC MODES FOR AN OPEN BOX CAVITY WITH ADJUSTABLE DEPTH

Steffen Hammer[1], Jens Fridh[2], Mattias Billson[3]

[1]KTH Royal Institute of Technology
[2]KTH Royal Institue of Technology
[3]GKN Aerospace Sweden

Abstract

Aerospace engineers are facing increased challenges in designing the next generation of aero engines. Engines need to be lighter, compact, more powerful and consume less fuel. On the other hand the designs are supposed to be more reliable than before. Modern compressors in those engines are playing a big role in fulfilling parts of these requirements by increased aerodynamic efficiency. Additionally, increasing requirements on compactness forcing new designs that may alter the acoustic resonance picture significantly. All these design adjustments face additional risks of component damage or fatigue. Air bleed systems are necessary parts in the compressor section of an aero engine to allow a wider operational range. However, these bleed systems can additionally introduce acoustic resonance due to the nature of air flow over an opening. The bleed design needs to be adapted to avoid this kind of resonance as much as possible. This paper is a continuation of an experimental investigation of cavity resonance for an open box cavity. The operating range covers the typical flow speeds in aero engine low pressure compressors. The geometry of a compressor bleed system is simplified to allow the use of theoretical prediction models. The previous results of detected acoustic resonances are screened for critical modes in terms of amplitude. This screening identified vulnerable operating points at higher Mach numbers in the range of 0.65 to 0.8 for all cavity length to depth ratios between 4 and 0.5. The test data show that an interaction of Rossiter modes with other feedback mechanisms can significantly amplify the acoustic resonance.

Keywords: Rossiter, Acoustic, Cavity, Bleed, Compressor

1. Introduction

The flow over an open cavity and its related acoustic resonances have been studied for a long time. Rossiter was the first to establish a detailed mathematical prediction model based on empirical data [1]. Rossiter suggested two constants (K=0.57 and γ=0.25) in his model to define shear layer modes that matched his empirical data. These mean values have been widely accepted and used over the years in several studies. Rockwell and Naudascher concluded in their studies on cavity shear layers in regards to resonance oscillations that a purely empirical model is not satisfactory to predict the frequencies of cavity oscillations [2]. Delprat challenges these accepted mean values and suggests to adjust them according to the depth of the cavity [3] for a better prediction and matching with measurement data. These suggestions go in line with the reports from Plentovich et al. who concluded that the transition of the flow behavior is dependent on cavity geometry and flow speeds [4]. This is especially of importance since several attempts have been made with the increase in computational power to build numerical models for the prediction of acoustic cavity resonances [5], [6]. Forestier et al. mentioned the challenge of matching CFD to existing experimental databases [7] while they only focused on two cavity depths and one high sub-sonic Machnumber. The accurate prediction of constant modes at one operating point might already be challenging, but the switching between different modes as reported by Rossiter [1] and Kegerise [8] increases this challenge even further. The importance of accurate prediction models is necessary since compressor bleed systems represent open cavities. Aleksentsev et al. presented that acoustic resonances in such systems may create challenges for the structural integrity of nearby components [9].

The focus of this present work is to further increase the understanding of measurement data for flow over an open box cavity for low to high-subsonic flow speeds. The length to depth ratios are herein in the range of 4 (shallow) up to 0.5 (deep) [10].

2. Experimental Method

The data presented in this paper is part of an experimental study to quantify the flow over a cavity of adjustable depth. A shear layer instability is created at the leading edge of the cavity due to the approaching flow. Meanwhile, the cavity is acting as an acoustic resonator. The interaction of the shear layer instability with other present acoustic resonances is the main research interest in relation to the cavity geometry. The results of the experiments shall help with numerical analyses in bleed cavities in the compressor section of an aero engine. The different cavity dimensions in the study represent geometric simplifications of these bleed cavities. Additionally, the operating points for the experiments are chosen to fulfil the typical range of free stream velocities in an aero engine.

2.1 Wind-Tunnel Facility

The experimental studies are carried out in an open wind tunnel facility as described in [10]. A 1MW electric motor is connected with a screw compressor which provides the required air flow during the experiments. A heat exchanger allows to adjust the temperature of the flow. A plate with an orifice is positioned downstream of the heat exchanger to quantify the effective mass flow entering the test section. In this interchangeable test section the mass flow and pressure are controlled with valves upstream and downstream the test section. The interchangeable test section consists of a round settling chamber followed by a rectangular tube. The cross section of this tube is 250 mm by 250 mm. The walls of the tube are first horizontally and then vertically converging to the measurement section with straight sidewalls. The measurement channel is 120 mm high and 100 mm wide. This channel is modular with access from four sides. This allows to include different test objects, optical windows and different kinds of instrumentation.

2.2 Cavity Model

For this study a plate (length = 290 mm, width = 100 mm) is installed at the lower wall of the modular measurement channel. A square open box (length = L, width = 1.5*L) is located centrally with its leading edge 3.125*L downstream the leading edge of the plate. Square plugs are used to adjust the depth (D) of the cavity to ratios of L/D of four, one and 0.5 as seen in Figure 1.

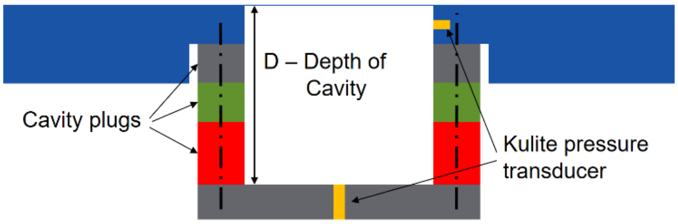

Figure 1 – Cavity schematic [10]

2.3 Instrumentation

9 unsteady pressure transducers (Kulites) are used during the measurements as seen in Figure 2. All Kulites are flush mounted. The cavity itself is equipped with one Kulite centrally at the bottom and on Kulite at the downstream wall. The downstream wall sensor is placed centrally in the width of the cavity and 5 mm below the cavity opening (Figure 1). The additional seven Kulites are placed downstream the cavity trailing edge in 15mm increments. Five Kulites are centrally fixed behind each other. Two transducers are mounted 15mm left and right of the centerline closest to the cavity trailing edge as shown in Figure 2.

Around the measurement channel several pressure taps are placed to be able to define the operating conditions. A pitot tube is place in the settling chamber to measure the total pressure. Three static pressure taps are placed 15 mm upstream the cavity leading edge in a line. The taps are located in the hub section of the measurement channel which includes the cavity. Each of these taps is 15 mm apart from each other with the middle one being in the center of the channel width. Additionally a pressure tap is placed in the side window at mid channel height and in the center of the cavity in flow direction. This tap is used to define the operating point together with the total pressure measurement from the settling chamber.

The last tap is placed centrally at the shroud downstream the measurement channel.

A 16-channel pressure acquisition system [11] is used to record the measurement from all taps simultaneously. The Kulite data is acquired with a DTS SLICE PRO acquisition system and a Windows PC. The unsteady measurements are sampled with 25 kHz and 50 kHz for a 4 second recording.

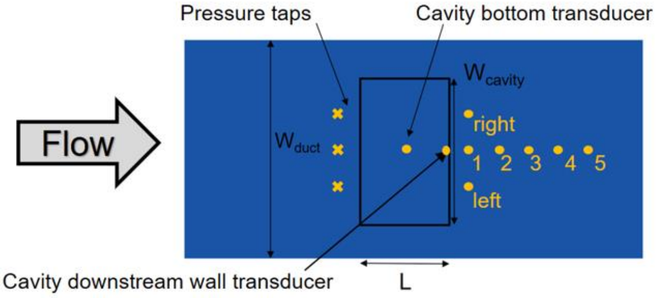

Figure 2 – Schematic top view of cavity with instrumentation [10]

2.4 Test Conditions

The free stream velocity in typical aero engine compressor sections reaches up to high subsonic Mach numbers. For these experiment the operating points are therefore between Mach 0.3 and 0.8. These flow speeds and the chosen geometry simplify a comparison with other published data [12]. The Mach number steps is chosen to be 0.02 within the operating range. In an attempt to identify specific lock-in frequencies [12] each of the three cavity depth models is measured twice at the various operating points. During the first of these test the flow speed is increased and in the second it is decreased.

The different cavity depth ratios are using the same inlet conditions of 116.7 kPa (+/- 0.3%) and 30° C within 0.5 K.

The operating point is established using the total pressure of the settling chamber and the static pressure at the side window with equation (1).

$$M = \left[\frac{2}{\gamma - 1} \times \left[\left(\frac{p_{tot\_settling}}{p_{s\_window}}\right)^{\frac{\gamma-1}{\gamma}} - 1\right]\right]^{\frac{1}{2}} \qquad (1)$$

2.5 Acoustic resonance models

Figure 3 shows schematically the half and quarter wavelength resonances to identify geometry induced resonances during the test. They are mathematically represented with equations 3, 4 and 5. Further, Rossiter modes are calculated with equation 2. Important for the Rossiter formula are the two constants K and γ. Rossiter defined these constants empirically to the mean values of K=0.57 and γ=0.25. However, Delprat mentions that adjusting K up to 0.66 can improve the prediction of the Rossiter modes depending on the cavity depth [3]. Therefore the Rossiter modes are plotted in the following figures as a range using values of K between 0.57 and 0.66, while keeping γ at 0.25 as proposed by Rossiter.

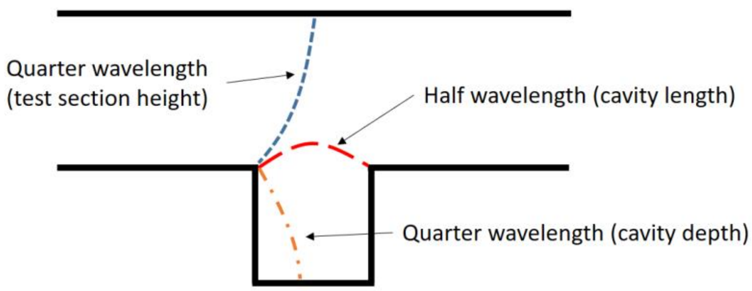

Figure 3 – Schematic of the test section with half and quarter wavelength resonator identified

Rossiter resonance

$$f = \frac{U(m-\gamma)}{U\left(\frac{1}{K} + M\right)} \qquad K = 0.57 - 0.66, \gamma = 0.25 \qquad (2)$$

Cavity length resonance

$$f = \frac{c}{2L} n \qquad n = 1,2,.. \qquad (3)$$

Test section height resonance

$$f = \frac{c}{4H}(2n-1) \qquad n = 1,2,.. \qquad (4)$$

Cavity depth resonance

$$f = \frac{c}{4D}(2n-1) \qquad n = 1,2,.. \qquad (5)$$

3. Results

In the following section the post-processed unsteady pressure measurements for three different depths of the open box cavity are presented.

A fast Fourier transformation (FFT) is applied to the time signal of the unsteady pressure measurements. Furthermore, the Fourier transforms are used to calculate the power spectrum density of the signal, with a frequency resolution of 24.6Hz.

In the following figures two plots are present for each cavity ratio using the signal from the Kulite mounted in the downstream cavity wall. Figure 4 [10] shows up to three measured modes with the highest amplitude for each operating point disregarding harmonics. Further, Rossiter [1] (equation 2), half and quarter wavelength resonances (equations 3, 4 and 5) are plotted as Strouhal number per operating point. In contrast, Figure 5 plots the same data as is a contour of operating points over frequency with power spectral density (PSD) as the amplitude. Using the contour plots allows to distinguish the frequencies with the highest amplitudes in the whole operating range. Furthermore, plotting frequencies on the y-axis allows to identify resonances created by the geometry, since they are seen as near horizontal lines. The slight downwards trend of these lines is an effect from the change in speed of sound. The static temperature drops with increasing Mach number which in return changes the speed of sound.

Additionally, the three Rossiter modes are shown as a range by changing K (0.57-0.66) between the most used values shown in literature [3].

Several acoustic modes are detected over the whole operating range in Figure 4. However, Figure 5 shows that the most critical acoustic resonance is in the higher operating range between Mach 0.7 and 0.76 for a shallow cavity around 2000 Hz. The highest amplitude over the whole operating range is measured at Mach 0.74 with 22.95 kPa. These modes seem to follow the Rossiter mode 1 prediction but are close to the predicted test section height resonance as well. The second highest amplitude (20.94 kPa) is measured at Mach 0.8 and lies in the range of the Rossiter mode 2 prediction around 4700 Hz. All other modes identified in Figure 4 have a much lower amplitude and are therefore nearly indistinguishable in Figure 5.

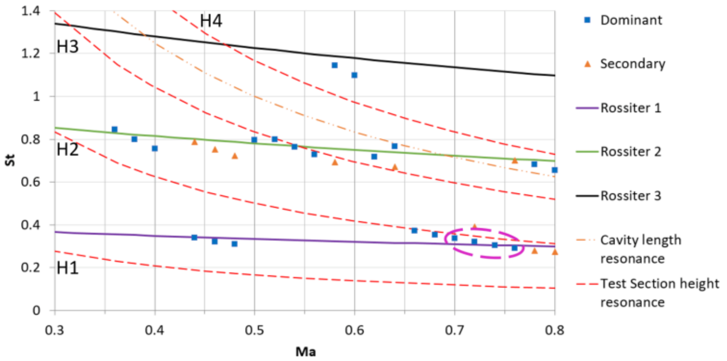

Figure 4 – Measured modes, computed Rossiter and other resonances for cavity L/D = 4, modified from [10]

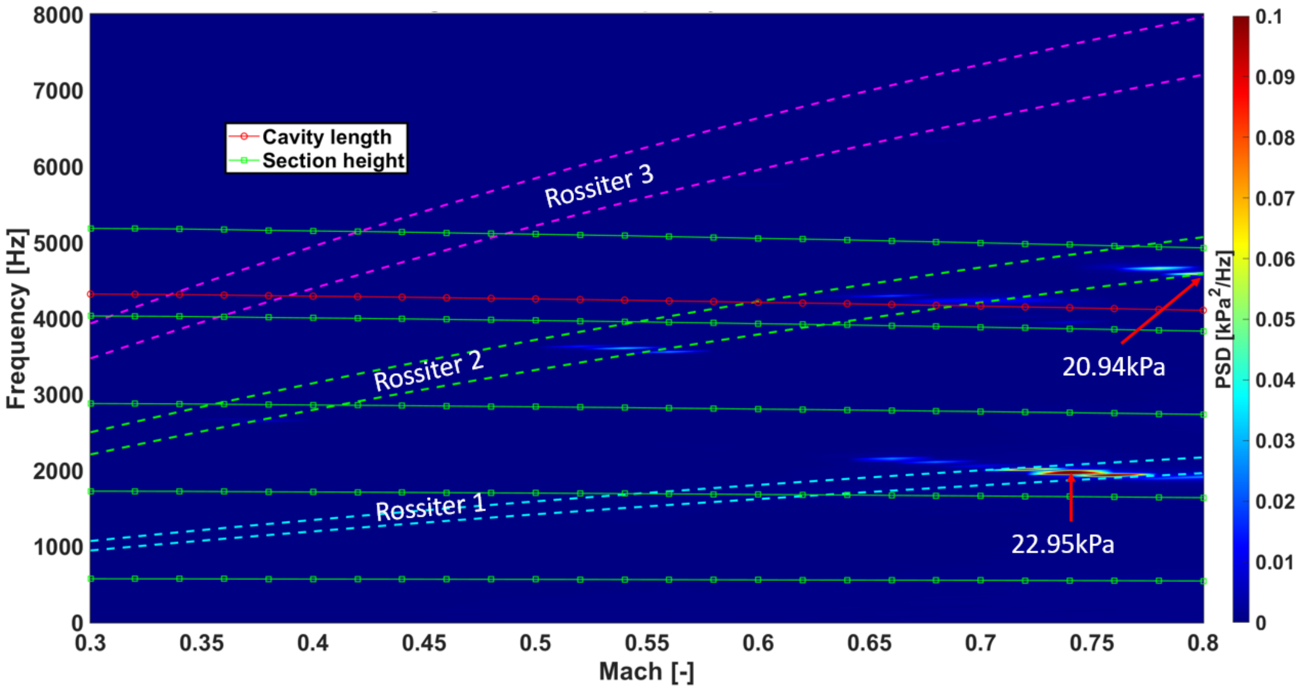

Figure 5 – Contour plot of PSD amplitude for measured modes for cavity L/D = 4

The results for the cavity with an L/D ratio of 1 are presented in Figure 6 and Figure 7. Similar to the shallow cavity with L/D=4 acoustic modes are measured over the whole operating range. However, for L/D =1 the modes appear at different Strouhal numbers/frequencies. The most critical modes in terms of amplitude are located between Mach 0.62 and 0.8 as shown in Figure 7. Figure 6 hints an amplification due to interaction with Rossiter mode 2 and the cavity length resonance. In the contour plot in Figure 7 and Figure 8 two unique resonances seem to appear in this operating range. From Mach 0.62 to 0.7 the resonance appears directly in the Rossiter mode 2 range. Further, the amplified frequency increases slightly (4500 Hz to 4700 Hz) with increasing operating points (Figure 8).
From Mach 0.7 to 0.8 the resonance stays at the same frequency level of about 4800 Hz. Although it is within the Rossiter mode 2 range, it also lies in between cavity length and test section height resonance prediction.
At Mach 0.62 a strong resonance lies in the Rossiter mode 3 prediction range but is also close to the harmonics of the test section height and cavity depth resonances around 6700 Hz.
Another distinguishable resonance in the contour plot appears between Mach 0.34 and 0.38 with a maximum amplitude of 7.3kPa around 1300 Hz. This is in contrast to the shallow cavity of L/D of 4 where the resonances in the lower operating range have a smaller amplitude. Although this resonance falls into the Rossiter mode 1 prediction, but it does not jump in frequency between the operating points.

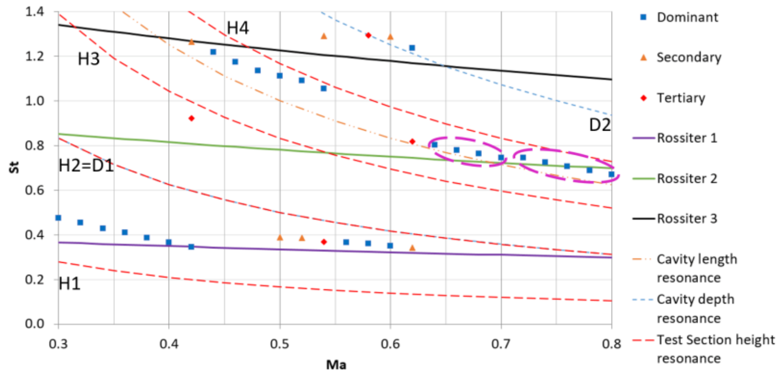

Figure 6 – Measured modes, computed Rossiter and other resonances for cavity L/D = 1, modified from [10]

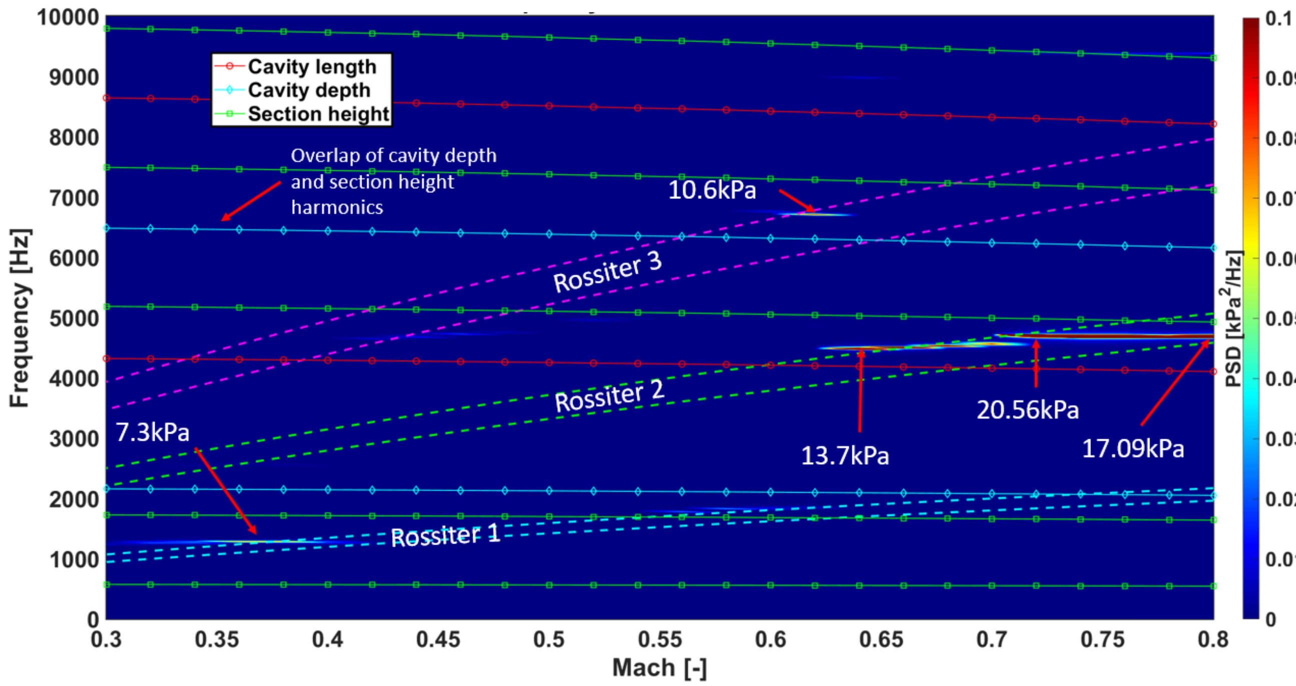

Figure 7 – Contour plot of PSD amplitude for measured modes for cavity L/D = 1

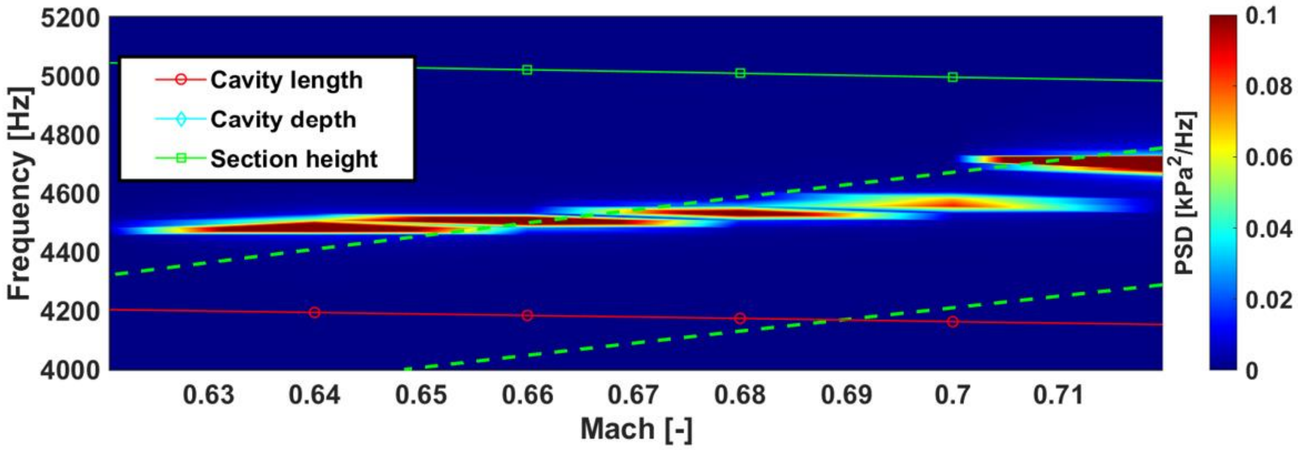

Figure 8 – Zoom into L/D = 1, M = 0.62 – 0.72

The results for the deepest cavity with an L/D ratio of 0.5 are shown in Figure 9 and Figure 10. Like Figure 6 acoustic modes can be identified over the whole operating range in similar locations. The contour in Figure 10 displays more regions with high amplitudes compared to the two shallower cavities. The peak amplitudes for these identifiable resonances range from 9.1 kPa to 22.2 kPa.
As for the intermediate cavity (L/D=1) stronger resonances appear in the range of lower Mach numbers. Although the operating range of the resonance is larger (M=0.3-0.42) for the deep cavity (L/D=0.5). The contour suggests two shifts in modes at Mach = 0.34 and 0.38 (around 800 Hz to 900 Hz). Which can indicate a shift from test section height to cavity depth resonance. On the other hand, this resonance behavior follows the same pattern as in the L/D=1 case and might be influenced by Rossiter mode 1. The strongest amplitude for this resonance is measured at Mach 0.36. This close to the intersection of Rossiter 1 and cavity depth resonance prediction as seen in Figure 9.
Another critical region is similar to the previous cavity (L/D=1) between Mach 0.66 and 0.72. Here the crossing between Rossiter mode 2 and the cavity length resonance occurs. Figure 10 shows the resonance as a horizontal line over several operating points around 4300 Hz. Further, the resonance is close to the cavity length resonance prediction.
The second strong amplification shows up directly in the Rossiter mode 2 range between Mach 0.74 and 0.78, but again as a horizontal line without any slope around 4800 Hz. It is close to the harmonic of the test section height resonance.
The highest amplitude is measured for a resonance between Mach 0.76-0.8 with 22.2 kPa around 2600 Hz. This region is aligned with the test section height prediction.
Between Mach 0.58-0.64 a strong resonance is picked up by the sensors around 2300 Hz with a maximum amplitude of 12.1 kPa but is not aligned with any of the included predictions. Additionally, there are other measured resonances that do not seem to follow any model. It could indicate an interaction of several resonance models that lead to these measurements.

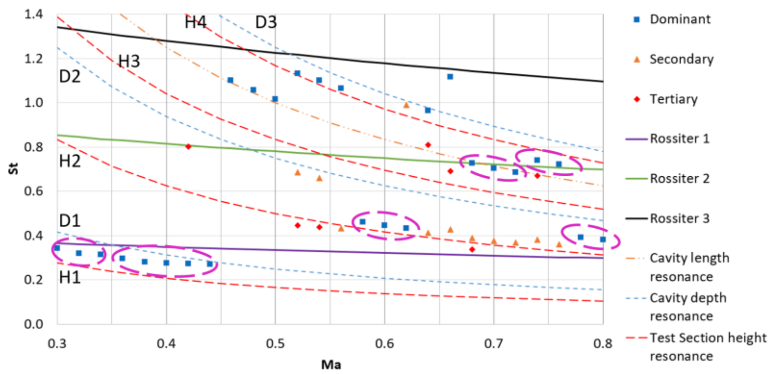

Figure 9 – Measured modes, computed Rossiter and other resonances for cavity L/D = 0.5, modified from [10]

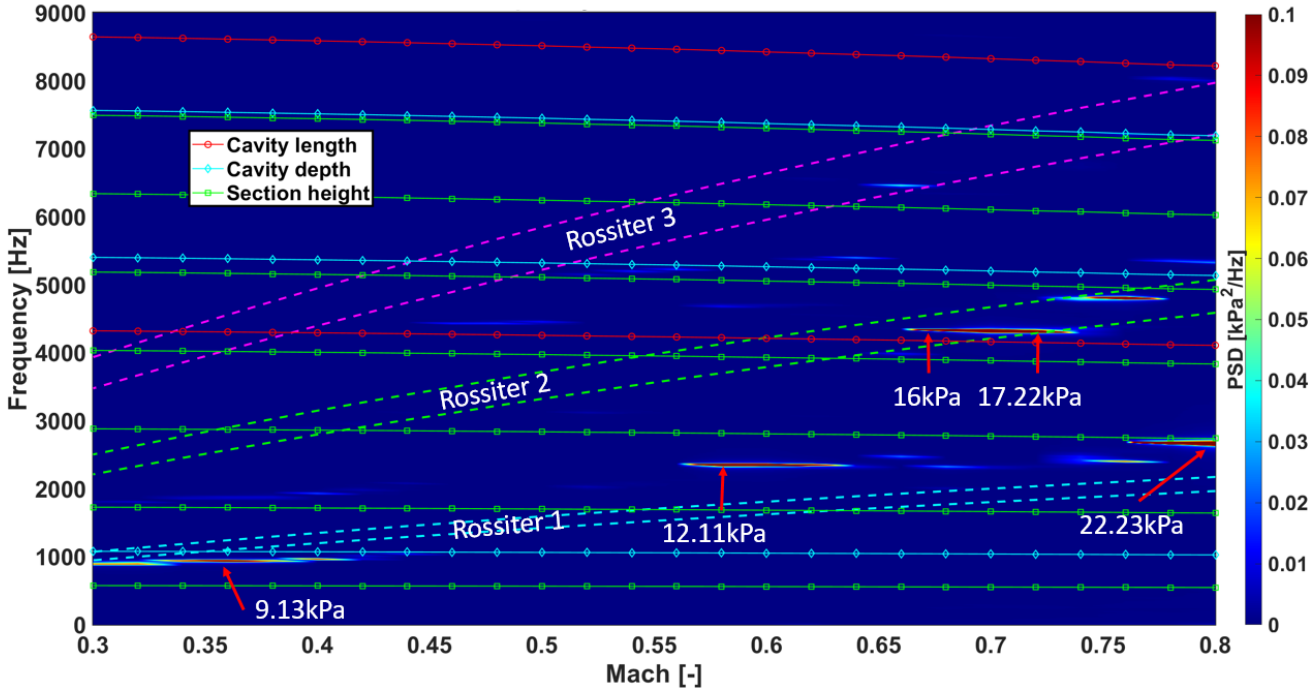

Figure 10 – Contour plot of PSD amplitude for measured modes for cavity L/D = 0.5

In Figure 11, Figure 12 and Figure 13 the highest amplitude for all sensors for the respective cavity length to depth ratio is shown. The data represents the measurements at Mach 0.74. This operating point is chosen since strong amplifications were measured for all L/D ratios.

The downstream wall sensor shows in all cases the highest amplitude with a similar level. For L/D = 4 and L/D = 1 the bottom place sensor measures the second highest amplitude level. For L/D = 0.5 the amplitude of the bottoms sensor is about equal to the 5 centrally located Kulites.

With increasing cavity depth the left and right placed Kulites show and increase in amplitude at this specific operating point. Additionally, the center-1 Kulite shows always the lowest amplitudes.

Table 1 presents the highest amplitude and its frequency for the downstream wall Kulite over the whole operating range. The table includes data for all 3 cavities presented above. The numbers in the table amplifiy the results of the contour plots that the strongest amplitudes are measured for Mach numbers greater than 0.68. However, the table also shows that at lower Mach numbers the amplitudes still reach up to 9 kPa.

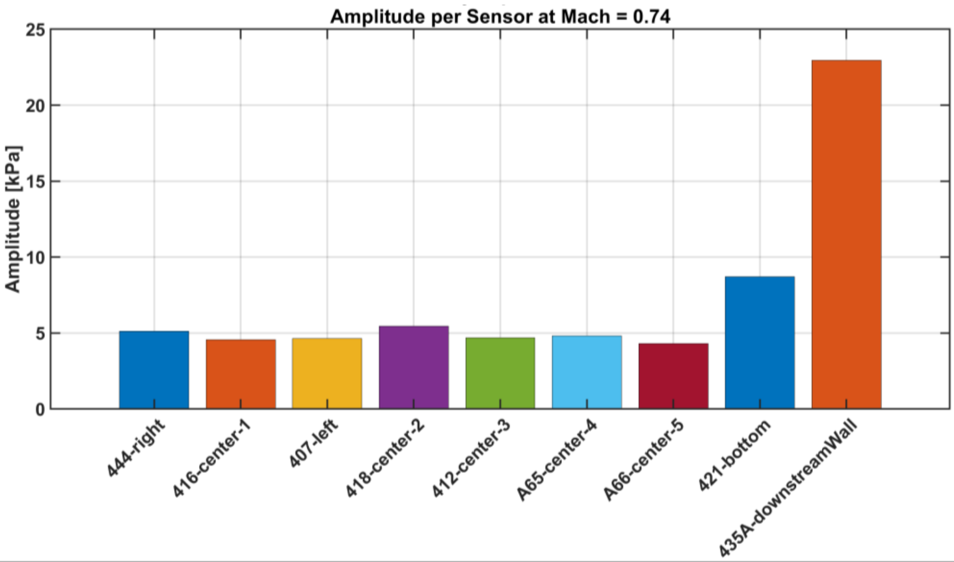

Figure 11 – Comparison of Pressure amplitude for all Sensors at M=0.74, L/D = 4

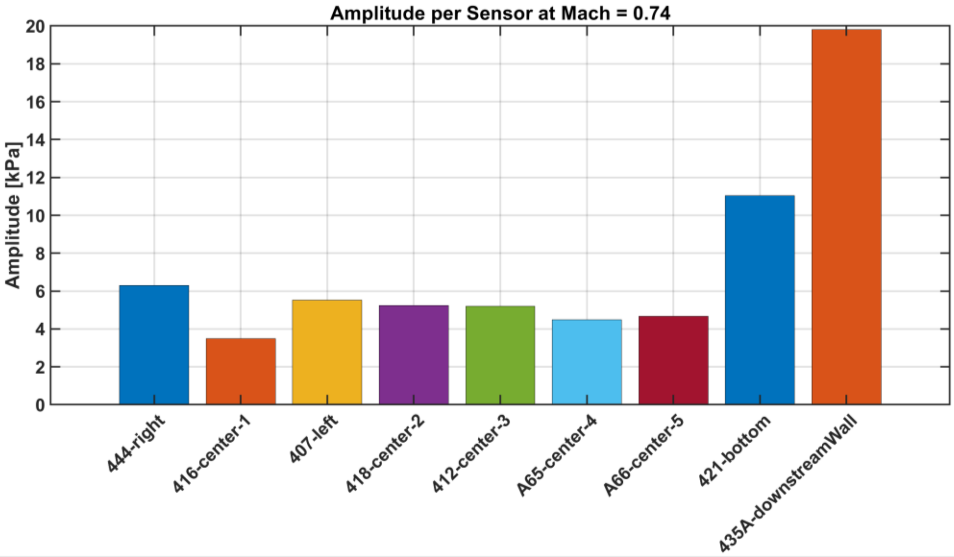

Figure 12 – Comparison of Pressure amplitude for all Sensors at M=0.74, L/D = 1

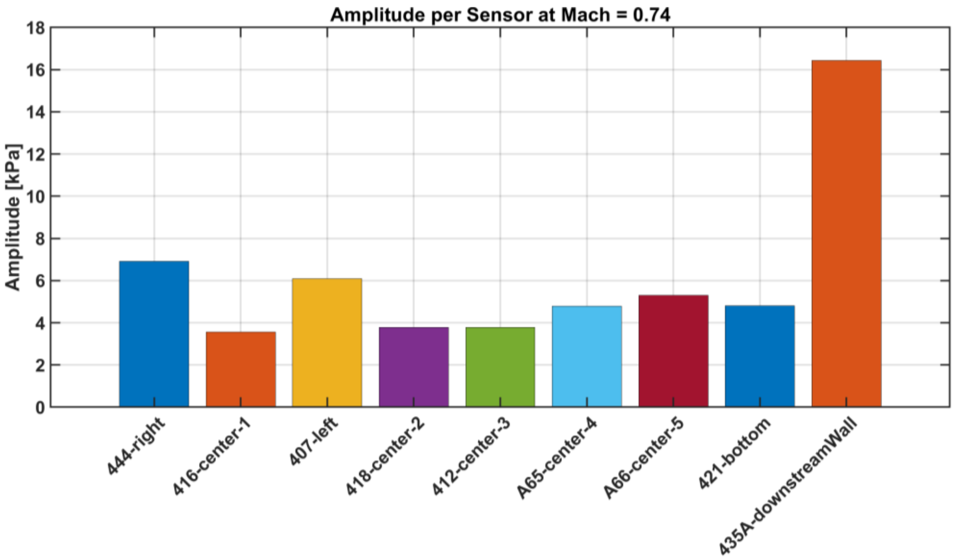

Figure 13 – Comparison of Pressure amplitude for all Sensors at M=0.74, L/D = 0.5

Table 1 – Frequencies with the highest measured amplitudes at the cavity downstream wall Kulite for all operating points and three L/D ratios

	L/D = 4		L/D = 1		L/D = 0.5	
Mach	Frequency [Hz]	Amplitude [kPa]	Frequency [Hz]	Amplitude [kPa]	Frequency [Hz]	Amplitude [kPa]
0.3	-	-	1238	3.81	892	7.08
0.32	-	-	1263	4.73	892	7.72
0.34	-	-	1288	5.53	941	7.7
0.36	2677	5.77	1288	6.37	941	9.13
0.38	2652	5.48	1288	7.31	941	8.96
0.4	2652	5.72	1288	6.41	966	8.56
0.42	-	-	4656	4.81	966	7.92
0.44	-	-	4681	4.98	1040	6.01
0.46	-	-	4730	5.14	4433	6.6
0.48	-	-	4755	5.26	4433	6.59
0.5	-	-	4879	4.39	4458	7.28
0.52	3635	10.85	4953	5.39	5151	7.07

0.54	3610	10.84	4978	5.59	5201	8.62
0.56	3561	10.01	1783	6.54	5225	9.68
0.58	5820	9.48	1833	7.75	2353	12.11
0.6	-	-	6761	8.44	2353	11.71
0.62	-	-	6711	10.64	2353	11.94
0.64	4298	11.91	4482	13.7	5399	10.34
0.66	2161	13.6	4507	13.06	6464	12.98
0.68	2112	15.71	4532	12.27	4334	16.01
0.7	2063	16.33	4557	11.09	4334	16.7
0.72	2014	17.14	4705	20.56	4309	17.22
0.74	1965	22.96	4681	19.81	4804	16.44
0.76	1940	19	4681	17.81	4804	16.87
0.78	4666	18.8	4681	16.46	2675	19.62
0.8	4592	20.94	4681	17.09	2675	22.23

4. Discussion

This study is performed to further understand the interaction of cavity resonances and Rossiter modes. The use of an open box cavity allows for an easier prediction of resonances created due to the geometry.

The presented results show clearly that the use of contour plots help to distinguish the strongest resonances over the operating range. However, it is also clear that seemingly lower amplitudes have a high magnitude. The use of frequencies over Strouhal numbers simplifies the identification of mode shifts. Furthermore, geometry induced resonances are easier to identify due to their near horizontal lines.

Rossiter modes can clearly be identified for L/D=4. The measured resonances are in the range of the Rossiter model and increase slightly with an increase in flow speed.

Interactions between Rossiter modes and geometric resonances appear for all L/D-ratios but for deeper cavities the number of resonances with higher amplitudes increases.

The above figures show that choosing the correct K value has clear significance for the mode identification. The contour plots with the Rossiter modes as a range confirms the necessity of the correct values for the Rossiter constants in regard to cavity depth. Especially for L/D = 0.5 the model needs to be updated. Rossiter did not give predictions for cavities with L/D ratios below one [3]. This is clearly noticeable in the figures since some of the measured amplitudes seem to follow the slope of a Rossiter mode but are not in the predicted range.

5. Conclusion

This study gives more insight on the previously analyzed data by highlighting the magnitude of measured resonance amplitudes. There are clear operating conditions with high amplitudes. However, in a real aero-engine application the nearby components and their structural behavior are values to consider as well in categorizing a critical frequency and its amplitude.

Interactions between Rossiter modes and geometric resonances happen. At several operating conditions the crossing of the predicted modes fall in line with high resonance amplitudes.

Further, the prediction models from Rossiter are a good match for cavity with L/D ratios of four and one. However, depending on the cavity depth the K parameter needs to be adjusted if a precise prediction model is to be build. Especially for the deepest cavity (L/D=0.5) the Rossiter mode prediction needs to be tuned for a better understanding of the observed resonances.

This is especially important since certain resonances are not yet understood. They do not match any of the predicted resonance models used in this study but appear to be connected to the geometry since they show up as horizontal lines.

6. Future works

The presented results increased the understanding of the measured acoustic resonances and can be used as a stepping stone to design methods to either reduce the measured amplitudes or move the resonance peaks. This can be done in consideration of design of nearby components in a compressor application.

Additionally, further or adjusted resonance models need to be considered to be able to fit the not matched measurement data. Herein a measurement of the acoustic resonance of the test section using loudspeakers can be an option.

The measurements will be used as baseline for numerical studies.

Finally, measurements of a cavity with increased geometric complexity will be performed.

7. Acknowledgements

The study has been funded by the Swedish Innovation Agency VINNOVA through the national aviation research programme NFFP. The authors want to gratefully acknowledge them for the technical and financial support given on the current work. Additionally, we want to thank our lab technician, Leif Pettersson, who has been involved to prepare the test setup and the department production engineering providing the EDM machining.

8. Contact Author Email Address

Steffen Hammer
KTH Royal Institute of Technology, Heat and Power Technology
Brinellvägen 68, 114 28 Stockholm, Sweden
Phone: +46764098167
mailto: steffenh@kth.se

9. Copyright Statement

References

[1] J. E. Rossiter, "Wind-Tunnel experiments on the flow over rectangular cavities at subsonic and transonic speeds," Ministry of Aviation, 1966.

[2] D. Rockwell och E. Naudascher, ”Review—Self-Sustaining Oscillations of Flow Past Cavities,” *Journal of fluids engineering,* vol. 100, pp. 152-165, 1978.

[3] N. Delprat, ”Rossiter's formula: A simple spectral model for a complex amplitude modulation process,” *Physics of Fluids,* vol. 18, 2006.

[4] E. B. Plentovich, M. B. Tracey och R. Stallings, ”Experimental cavity pressure measurements at subsonic and transonic speeds. Static-pressure results,” NASA Technical Report, 1993.

[5] G. A. Brès och T. Colonius, ”Three-dimensional instabilities in compressible flow over open cavities,” *J. Fluid Mech.,* vol. 599, pp. 309-339, 2008.

[6] T. Colonius, ”An overview of simulation, modeling and active control of flow/acoustic resonance in open cavities,” i *39th Aerospace Sciences Meeting and Exhibit*, Reno, NV, USA, 2001.

[7] N. Forestier, L. Jaquin och P. Geffroy, ”The mixing layer over a deep cavity at high-subsonic speed,” *J. Fluid Mech.,* vol. 475, pp. 101-145, 2003.

[8] M. A. Kegerise, ”Mode-switching and nonlinear effects in compressible flow over a cavity,” *Physics of Fluids,* vol. 16, 2004.

[9] A. Aleksentsev, A. Sazhenkov och S. Sukhinin, ”Acoustic Resonance Phenomena in Air Bleed Channels in Aviation Engines,” *Journal of Applied Mechanics and Technical Physics,* vol. 16, pp. 971-978, 2016.

[10] S. Hammer, J. Fridh och M. Billson, ”Experimental investigation of Rossiter modes for an opnen box cavity with adjustable depth,” i *Proceedings of ASME Turbo Expo 2021*, 2021.

[11] I. P. Systems, ”Model 9116 Intelligent Pressure Scanner User's Manual,” 2007.

[12] H. Plumblee, J. Gibson och L. Lassiter, ”A theoretical and experimental investigation of the acoustic response of cavities in an aerodynamic flow,” 1962.